LETTERS

Micrometre-scale silicon electro-optic modulator

Qianfan Xu[1], Bradley Schmidt[1], Sameer Pradhan[1] & Michal Lipson[1]

Metal interconnections are expected to become the limiting factor for the performance of electronic systems as transistors continue to shrink in size. Replacing them by optical interconnections, at different levels ranging from rack-to-rack down to chip-to-chip and intra-chip interconnections, could provide the low power dissipation, low latencies and high bandwidths that are needed[1–4]. The implementation of optical interconnections relies on the development of micro-optical devices that are integrated with the microelectronics on chips. Recent demonstrations of silicon low-loss waveguides[5–7], light emitters[8], amplifiers[9–11] and lasers[12,13] approach this goal, but a small silicon electro-optic modulator with a size small enough for chip-scale integration has not yet been demonstrated. Here we experimentally demonstrate a high-speed electro-optical modulator in compact silicon structures. The modulator is based on a resonant light-confining structure that enhances the sensitivity of light to small changes in refractive index of the silicon and also enables high-speed operation. The modulator is 12 micrometres in diameter, three orders of magnitude smaller than previously demonstrated. Electro-optic modulators are one of the most critical components in optoelectronic integration, and decreasing their size may enable novel chip architectures.

Highly compact electro-optical modulators have been demonstrated in compound semiconductors[14]. However, in silicon, electro-optical modulation has been demonstrated only in large structures[15–17], and is therefore inappropriate for effective on-chip integration. Electro-optical control of light on silicon is challenging owing to its weak electro-optical properties[18]. The large dimensions of previously demonstrated structures were necessary to achieve a significant modulation of the transmission in spite of the small change of refractive index of silicon[15–17,19,20]. Liu *et al.* have recently demonstrated a high-speed silicon optical modulator based on a metal–oxide–semiconductor (MOS) configuration[17]. Their work showed a high-speed optical active device on silicon—a critical milestone towards optoelectronic integration on silicon. However, owing to the weak dependence of silicon's refractive index on the electron–hole pair concentration, and the limited mode confinement in the active region of the MOS device, the devices in ref. 17 have relatively large lengths (of the order of millimetres).

Light-confining resonating structures can enhance the effect of refractive index change on the transmission response[21–23]. In ref. 23, silicon ring resonators were used for all-optical modulation. The optical properties of the device were changed by using one beam of light to optically inject electrons and holes and thus control the flow of another beam of light. Using the principle of high confinement, here we present a silicon electro-optical modulator of a few micrometres in size[24].

The schematic of the electro-optic modulator is shown in Fig. 1. The modulator consists of a ring resonator coupled to a single waveguide. The transmission of the waveguide is highly sensitive to the signal wavelength and is greatly reduced at wavelengths in which the ring circumference corresponds to an integer number of guided wavelengths[23,25]. By tuning the effective index of the ring waveguide, the resonance wavelength is modified, which induces a strong modulation of the transmitted signal. The effective index of the ring is modulated electrically by injecting electrons and holes using a p-i-n junction embedded in the ring resonator. Figure 1 (inset) shows the cross-section of this rib waveguide. It consists of a strip waveguide formed on a 50-nm-thick slab layer. Because the thickness of the slab is much smaller than the wavelength propagating in the device (~1.5 μm), the mode profile of this waveguide is very close to that of the silicon strip waveguide. The highly doped p- and n-regions are defined around the ring using ion implantation. Ohmic contacts are deposited on the doped regions. To minimize absorption losses, the doped regions are formed approximately 1 μm away from the ring resonator, ensuring that the overlap of the resonating mode with the doped regions is minimal[26].

We fabricated the p-i-n ring resonator on a silicon-on-insulator substrate with a 3-μm-thick buried oxide layer. Both the waveguide coupling to the ring and that forming the ring have a width of 450 nm and a height of 250 nm. The diameter of the ring is 12 μm, and the spacing between the ring and the straight waveguide is 200 nm. To ensure high coupling efficiency between the waveguide and the incoming optical fibre, nanotapers[27] are fabricated at the ends of the waveguide. The structures are defined using electron-beam lithography followed by reactive ion plasma etching. Figure 2a shows the top-view scanning electron microscopy (SEM) image of the ring coupled to the waveguide with a close-up inset of the coupling region. Following the etching, the n+ and p+ regions of the diode are each defined with photolithography and implanted with phosphorus and boron to create concentrations of 10^{19} cm^{-3}. A

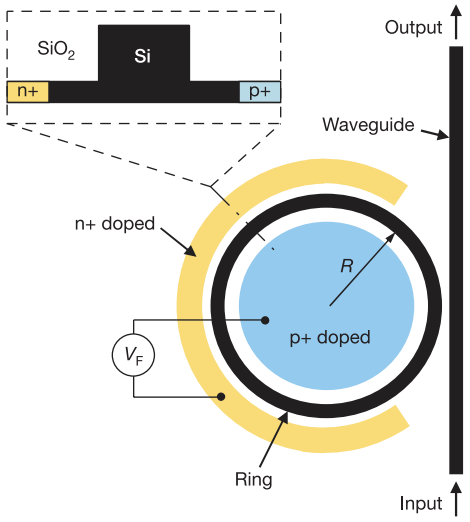

Figure 1 | Schematic layout of the ring resonator-based modulator. The inset shows the cross-section of the ring. *R*, radius of ring. V_F, voltage applied on the modulator.

[1]School of Electrical and Computer Engineering, Cornell University, 411 Phillips Hall, Ithaca, New York 14853, USA.

1-μm-thick silicon dioxide layer is then deposited onto the wafer using plasma-enhanced chemical vapour deposition followed by an annealing process to activate the dopants (15 s at 1,050 °C for p+ and 15 min at 900 °C for n+). Holes were patterned using photolithography and then etched down to the doped silicon regions, followed by evaporation and liftoff of the titanium contacts. Figure 2b shows the top-view microscope image of the ring resonator after the metal contacts are formed.

Continuous-wave light (dominant electric field parallel to the plane of the substrate) from a tunable laser is coupled to the waveguide adjacent to the ring, and the output spectrum of the waveguide is measured. The free-spectrum range of the ring resonator is 15 nm. Figure 3 shows the relative transmission through the modulator around the resonance of 1,574 nm at different bias values of the p-i-n junction. The total optical loss of the testing sample, including the coupling loss between the fibre and the waveguide, and the propagation loss in the 7.5-mm-long waveguide leading to the modulator, is about 9 dB. The solid curve shows the spectrum when the forward bias (0.59 V) on the p-i-n junction is much lower than the built-in potential of the junction, and the current through the junction is below our detection limit (0.1 μA). The spectrum shows a 15-dB drop in transmission at the resonant wavelength of 1,574.9 nm. The low transmission at this wavelength is the initial condition of a 'dark-to-light' intensity modulator. The 3-dB bandwidth of the resonance $\Delta\lambda$ is 0.04 nm measured from the spectrum, corresponding to a quality factor, defined as $Q = \lambda/\Delta\lambda$, of 39,350. This Q factor corresponds to a cavity photon lifetime of $\tau_{cav} = \lambda^2/(2\pi c\Delta\lambda) = 33$ ps, where c is the speed of light in vacuum. Thus, despite the resonant nature of the structure, the photon confinement of the modulator is not limiting its speed. The small ripples (~1 dB) on the waveform originate from the reflections at both ends of the waveguide, which can be eliminated by anti-reflection coating.

The electron–hole pair density in the cavity increases as the forward bias on the p-i-n junction increases. The dashed and dotted curves in Fig. 3 show the spectra when the bias voltage is 0.87 V and 0.94 V, and the current is 11.1 μA and 19.9 μA, respectively. In both cases the resonance is blue-shifted owing to the lowering of the effective index caused by the increase of the electron–hole pair density in the cavity[18]. The depths of the notches in the spectra decrease owing to the increased optical absorption in the ring induced by the electrons and holes. The extra absorption per round-trip in the ring is estimated from the spectra to be 0.03 dB at 0.87 V bias and 0.05 dB at 0.94 V bias. At the probe wavelength of 1,573.9 nm, we can see from Fig. 3 that 97% (15 dB) modulation can be obtained with less than 0.3-V bias voltage change. At this wavelength, because light does not couple to the ring when the electrons and holes are generated, the effect of the extra absorption in the ring on the modulation is less than 0.1 dB.

The light-confining nature of the modulator not only enables shrinking of the device size, but also enables high-speed operation under p-i-n configuration. The p-i-n configuration of the modulator, as opposed to the MOS configuration[17], is important for achieving high modulation depth, because the overlap between the region where the index is changed and the optical mode of the waveguide is large. However, p-i-n devices have traditionally been considered as relatively slow compared with MOS devices. In p-i-n devices, while extraction of electrons and holes in reverse-biased operation can be fast, down to tens of picoseconds[28], injection of electrons and holes in forward-bias operation is slow, which limits the rise time of the p-i-n to of the order of 10 ns, as measured in our device. The resonating nature of the modulator removes this speed limitation.

The inset in Fig. 3 shows the transfer function of the device, that is, the transmission of the modulator at the wavelength of 1,573.9 nm with different bias voltages. This transfer function shows that the resonating nature of the device enables voltages larger than 0.9 V to be applied without modifying the optical transmission ($T \approx 1$). This is because at these voltages, the resonance of the device is completely detuned from the probe wavelength. This insensitivity of the optical transmission at higher bias voltage is in strong contrast to Mach–Zehnder modulators, in which higher voltage strongly affects the transmission. When the device is operated at higher voltages, the optical transmission can reach ~1 well before the p-i-n junction reaches its steady state. This means that the optical rise time can be far less than the electrical rise time of ~10 ns with high forward bias, which is crucial for achieving high-speed modulation.

To measure the dynamic response of the modulator, electrical signals generated by a pulse-pattern generator and a wideband microwave amplifier are used to drive a modulator. The output of the waveguide is sent to a 12-GHz detector and the waveform is recorded on an oscilloscope. Figure 4a, b shows the waveform of both the driving signal using a non-return-to-zero (non-RZ) pattern and the optical output, demonstrating high modulation depths at 0.4 Gbit s^{-1}. The peak-to-peak voltage (V_{pp}) of the driving signal is 3.3 V, from −1.85 V to +1.45 V. The speed of the device is limited by the fact that the p-i-n junction is formed on only part of the ring resonator (see Fig. 1). During the forward-biasing period, electrons and holes diffuse into the section of the ring that is not part of the p-i-n junction (the section close to the straight waveguide),

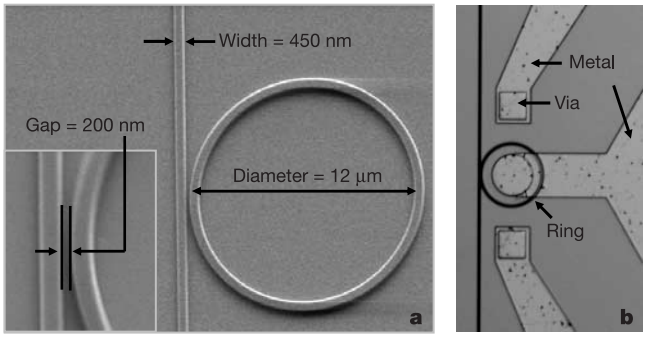

Figure 2 | SEM and microscope images of the fabricated device. a, Top-view SEM image of the ring coupled to the waveguide with a close-up view of the coupling region. **b**, Top-view microscope image of the ring resonator after the metal contacts are formed. The metal contact on the central p-doped region of the ring goes over the ring with a 1-μm-thick silicon dioxide layer between the metal and the ring.

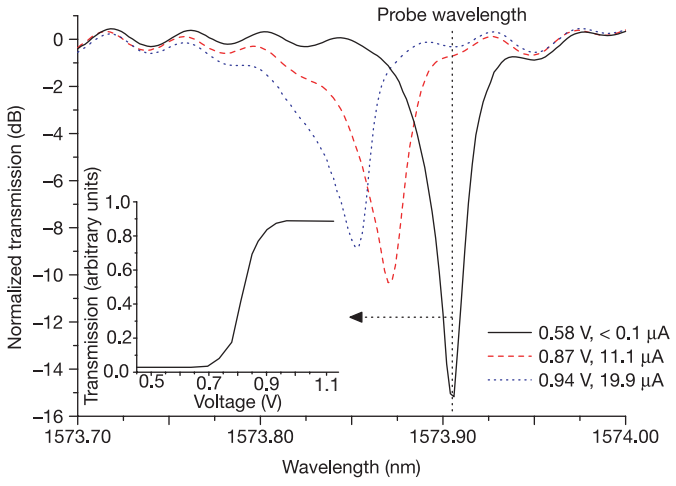

Figure 3 | DC measurement of the ring resonator. The main panel shows the transmission spectra of the ring resonator at the bias voltages of 0.58 V, 0.87 V, and 0.94 V, respectively. The vertical dashed line marks the position of the probe wavelength used in the transfer function and dynamic modulation measurements. The inset shows the transfer function of the modulator for light with a wavelength of 1,573.9 nm.

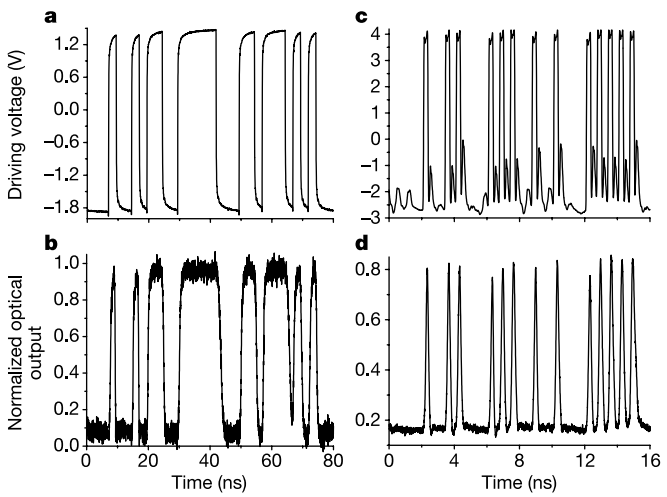

Figure 4 | Waveforms of the electrical driving signal and the transmitted optical signal. a, Waveform of the 32-bit pseudo-random non-RZ signal at 0.4 Gbit s^{-1} applied on the modulator. **b**, Waveform of the output optical power of the modulator with non-RZ modulation, normalized to the output power when the ring resonator is completely out of resonance. **c**, Waveform of the 127-bit pseudo-random bit sequence RZ signal at 1.5 Gbit s^{-1} applied on the modulator with a microwave amplifier. **d**, Waveform of the normalized output optical power of the modulator with RZ modulation.

where they cannot be efficiently extracted during the reverse-biased period, leading to a longer fall time (~1.5 ns) following long forward-biasing periods. This longer fall time is determined by the intrinsic lifetime of the electrons and holes in the non-p-i-n region and is independent of the reverse-biased voltage.

Figure 4c, d shows high modulation depths of the device at 1.5 Gbit s^{-1}. The modulator is driven by a 1.5 Gbit s^{-1} RZ signal with $V_{pp} = 6.9$ V (from −2.8 V to +4.1 V). The RZ signal does not have a long forward-biasing period, so the diffusion of electrons and holes into the non-p-i-n region is reduced. This enables the device to work at a higher bit-rate, despite the fact that the RZ signal generally requires twice as much bandwidth as the non-RZ signal for the same bit-rate. The higher voltage swing allows faster injection and extraction of electrons and holes, and the rise time and fall time of the optical output are found to be 200 ps and 150 ps, respectively. Note that, owing to the step-like transfer function of the modulator, the optical output does not follow the distortion of the electrical signal caused by reflections in the electrical driving system.

The driving voltage of the modulator can be decreased by reducing the contact resistance (currently ~4 kΩ). Using a typical value of ~100 Ω (ref. 29), the voltage drop on the contact resistance, estimated to be ~4 V_{pp} in the RZ-driven experiment, can be reduced to ~0.1 V_{pp}. We estimate that the silicon ring resonator, with the p-i-n junction covering the whole ring and low contact resistance, can be modulated at a bit-rate higher than 5 Gbit s^{-1} with a non-RZ signal of ~3 V_{pp}.

The wavelength-selective modulation property of the modulator can be used for building wavelength division multiplexing (WDM) interconnections, which can greatly extend the bandwidth of optical interconnections. Given the short length of the modulator (<20 μm) and the waveguide propagation loss of 4 ± 1 dB cm^{-1} (refs 6, 7), the insertion loss of the modulator is negligible to light with wavelength detuned from the ring resonance. The small insertion loss of the modulator makes it possible to cascade multiple modulators along a single waveguide and modulate each WDM channel independently. Note that this implementation would require the dimensions of the ring resonators to be controlled such that the resonant wavelength of each ring resonator equals the wavelength of the corresponding WDM channel.

Received 8 February; accepted 22 March 2005.

1. Miller, D. A. B. Optical interconnects to silicon. *IEEE J. Sel. Top. Quant. Electron.* **6,** 1312–1317 (2000).
2. Meindl, J. D. *et al.* Interconnect opportunities for gigascale integration. *IBM Res. Dev.* **46,** 245–263 (2002).
3. Mohammed, E. M. *et al.* Optical I/O technology for digital VLSI. *Proc. SPIE* **5358,** 60–70 (2004).
4. Kibar, O., Van Blerkom, D. A., Fan, C. & Esener, S. C. Power minimization and technology comparisons for digital free-space optoelectronic interconnections. *J. Lightwave Technol.* **17,** 546–555 (1999).
5. Lee, K. K., Lim, D. R. & Kimerling, L. C. Fabrication of ultralow-loss Si/SiO_2 waveguides by roughness reduction. *Opt. Lett.* **26,** 1888–1890 (2001).
6. Vlasov, Y. A. & McNab, S. J. Losses in single-mode silicon-on-insulator strip waveguides and bends. *Opt. Express* **12,** 1622–1631 (2004).
7. Dumon, P. *et al.* Low-loss SOI photonic wires and ring resonators fabricated with deep UV lithography. *IEEE Photon. Technol. Lett.* **16,** 1328–1330 (2004).
8. Chan, S. & Fauchet, P. M. Silicon microcavity light emitting devices. *Opt. Mater.* **17,** 31–34 (2001).
9. Jones, R. *et al.* Net continuous wave optical gain in a low loss silicon-on-insulator waveguide by stimulated Raman scattering. *Opt. Express* **13,** 519–525 (2005).
10. Espinola, R. L., Dadap, J. I., Osgood, R. M., McNab, S. J. & Vlasov, Y. A. Raman amplification in ultrasmall silicon-on-insulator wire waveguides. *Opt. Express* **12,** 3713–3718 (2004).
11. Xu, Q., Almeida, V. R. & Lipson, M. Time-resolved study of Raman gain in highly confined silicon-on-insulator waveguides. *Opt. Express* **12,** 4437–4442 (2004).
12. Boyraz, O. & Jalai, B. Demonstration of a silicon Raman laser. *Opt. Express* **12,** 5269–5273 (2004).
13. Rong, H. *et al.* An all-silicon Raman laser. *Nature* **433,** 292–294 (2005).
14. Sadagopan, T., Choi, S. J., Dapkus, P. D. & Bond, A. E. *Digest of the LEOS Summer Topical Meetings* MC2–3 (IEEE, Piscataway, New Jersey, 2004).
15. Tang, C. K. & Reed, G. T. Highly efficient optical phase modulator in SOI waveguides. *Electron. Lett.* **31,** 451–452 (1995).
16. Dainesi, P. *et al.* CMOS compatible fully integrated Mach–Zehnder interferometer in SOI technology. *IEEE Photon. Technol. Lett.* **12,** 660–662 (2000).
17. Liu, A. *et al.* A high-speed silicon optical modulator based on a metal-oxide-semiconductor capacitor. *Nature* **427,** 615–618 (2004).
18. Soref, R. A. & Bennett, B. R. Electrooptical effects in silicon. *IEEE J. Quant. Electron.* **23,** 123–129 (1987).
19. Gan, F. & Kärtner, F. X. High-speed silicon electro-optic modulator design. *IEEE Photon. Technol. Lett.* (in the press).
20. Sciuto, A., Libertino, S., Alessandria, A., Coffa, S. & Coppola, G. Design, fabrication, and testing of an integrated Si-based light modulator. *J. Lightwave Technol.* **21,** 228–235 (2003).
21. Heebner, J. E. *et al.* Enhanced linear and nonlinear optical phase response of AlGaAs microring resonators. *Opt. Lett.* **29,** 769–771 (2004).
22. Maune, B., Lawson, R., Gunn, C., Scherer, A. & Dalton, L. Electrically tunable ring resonators incorporating nematic liquid crystals as cladding layers. *Appl. Phys. Lett.* **83,** 4689–4691 (2003).
23. Almeida, V. R., Barrios, C. A., Panepucci, R. R. & Lipson, M. All-optical control of light on a silicon chip. *Nature* **431,** 1081–1084 (2004).
24. Pradhan, S., Almeida, V. R., Barrios, C. & Lipson, M. *Optical Amplifiers and Their Applications / Integrated Photonics Research Topical Meetings* IWA5 CD-ROM (The Optical Society of America, Washington, DC, 2004).
25. Little, B. E. *et al.* Ultra-compact $Si-SiO_2$ microring resonator optical channel dropping filters. *IEEE Photon. Technol. Lett.* **10,** 549–551 (1998).
26. Barrios, C. A., Almeida, V. R., Panepucci, R. & Lipson, M. Electrooptic modulation of silicon-on-insulator submicrometer-size waveguide devices modulator. *J. Lightwave Technol.* **21,** 2232–2239 (2003).
27. Almeida, V. R., Panepucci, R. R. & Lipson, M. Nanotaper for compact mode conversion. *Opt. Lett.* **28,** 1302–1304 (2003).
28. Muller, J. Thin silicon film p-i-n photodiodes with internal reflection. *IEEE J. Solid-State Circ.* **13,** 173–179 (1978).
29. Faith, T. J., Irven, R. S., Plante, S. K. & O'Neill, J. J. Contact resistance: Al and Al-Si to diffused N+ and P+ silicon. *J. Vac. Sci. Technol. A* **1,** 443–448 (1983).

Acknowledgements This work has been partially carried out as part of the Interconnect Focus Center Research Program at Cornell University, supported in part by the Microelectronics Advanced Research Corporation (MARCO), its participating companies, and DARPA. We acknowledge support by the National Science Foundation (NSF). We thank G. Pomrenke, AFOSR, for supporting the work. We also acknowledge support by the Cornell Center for Nanoscale Systems. The devices were fabricated at the Cornell Nano-Scale Science & Technology Facility. We also thank J. Shah, DARPA, for funding this work as part of the EPIC programme.

Author Information Reprints and permissions information is available at npg.nature.com/reprintsandpermissions. The authors declare no competing financial interests. Correspondence and requests for materials should be addressed to M.L. (lipson@ece.cornell.edu).